Chapter 5

Sulfur K-edge X-ray absorbance spectroscopy of the 4Fe4S cluster of Endonuclease III with DNA*

*Experiments done in collaboration with Yang Ha of the Solomon and Hodgson groups at Stanford University. A.R.A. prepared the samples; Y.H. measured samples and processed the data.

5.1 Introduction

Endonuclease III (EndoIII) is a glycosylase enzyme that excises oxidized pyrimidines as part of the base excision repair (BER) pathway in order to maintain the integrity of genomic DNA (*1*). EndoIII contains a $[4Fe4S]^{2+}$ cluster as-isolated (Figure 1) that is relatively insensitive to reduction and oxidation in solution (*2*), leading to a proposed structural role for the cluster although it is not required for folding or stability in the homologous BER enzyme MutY (*3*). However, we have found electrochemically that the redox potential of the EndoIII cluster shifts upon DNA binding (*4*). Here, we form DNA monolayers on electrode surfaces and then monitor the electrochemistry of a DNA-bound redox probe through DNA charge transport (CT). In this process, charge is funneled from the electrode surface through the π-stack of the DNA bases to reach the redox probe, which must be electronically coupled to the DNA π-stack (*5*). The redox probe can be an intercalating organic dye, such as nile blue or methylene blue, or a redox-active DNA-binding protein (*5*).

Specifically, we have measured the electrochemistry of *E. coli* EndoIII on highly ordered pyrolytic graphite (HOPG) electrodes that were either bare or modified with mixed-sequence 15-mer DNA. When EndoIII was investigated on a bare HOPG electrode, two signals were observed: an irreversible anodic peak at 250 mV and a cathodic peak at -300 mV, assigned to the $[4Fe4S]^{3+/2+}$ and $[4Fe4S]^{2+/1+}$ couples, respectively (*4*). Conversely, on DNA-modified HOPG electrodes, a single redox couple with a midpoint potential of 20 mV versus NHE was observed. This quasi-reversible redox signal was assigned to the $[4Fe4S]^{3+/2+}$

couple of EndoIII. A similar midpoint potential was observed on DNA-modified gold electrodes (*6*). Thus according to these electrochemistry results, DNA binding of EndoIII negatively shifts the $[4Fe4S]^{3+/2+}$ redox potential of the cluster by at least 200 mV, activating the cluster towards oxidation (*4*). Generally, the redox potential of iron-sulfur clusters is sensitive to the protein environment, with the major factors being solvent accessibility, hydrogen bonding, and electrostatics (*7*). The factors most likely involved in the negative shift in potential of the 4Fe4S cluster of EndoIII upon DNA binding are: (*i*) a more buried, less solvent-accessible cluster environment, and (*ii*) the electrostatics of the DNA poly-anion. The redox potential of DNA-bound EndoIII is high potential iron-sulfur protein (HiPIP)-like, given that the $[4Fe4S]^{3+/2+}$ couple has been shifted into a physiologically relevant range (*6*).

Other DNA processing enzymes have been discovered with similar DNA-bound $[4Fe4S]^{3+/2+}$ redox potentials of approximately 80 mV versus NHE. These include the BER proteins MutY and UDG (*6*), the nucleotide excision repair helicase XPD (*8*), and the helicase DinG shown to be involved in R-loop maturation (*9*). Additionally, because significant conformational changes do not occur upon the DNA binding of EndoIII, a thermodynamic consequence of the approximately 200 mV negative shift in redox potential is that the oxidized, $[4Fe4S]^{3+}$, form of EndoIII has a much higher affinity for DNA (3 orders of magnitude) than the reduced, $[4Fe4S]^{2+}$, form (*4*). Combined with the fast kinetics of DNA CT (picoseconds) (*10*), these observations suggested a model whereby these often low-copy number enzymes could use DNA CT to cooperate inside cells to efficiently localize

to the vicinity of lesions (*11*). Essentially, this proposed model consists of long-distance DNA-mediated electron transfer self-exchange reactions between two 4Fe4S cluster proteins with similar DNA-bound redox potentials. When the DNA intervening between the two proteins is undamaged, the self-exchange reaction can proceed efficiently, with the result that one of the DNA-bound proteins is reduced and its affinity for DNA lowered. This protein can then diffuse to another region of the genome. However, in the case of an intervening mismatch or lesion that disrupts π-stacking and attenuates DNA CT, this self-exchange reaction is inhibited. Both proteins would remain bound to the DNA in the vicinity of the lesion, significantly reducing the range over which the slower process of diffusion must occur.

While we have shown the redox potential shift of the 4Fe4S cluster of EndoIII upon DNA binding electrochemically, these experiments do not provide direct molecular evidence for the species being observed. The goal of this work is to use spectroscopic methods to directly monitor changes in the iron-sulfur cluster upon DNA binding in order to obtain this direct molecular evidence for the redox potential shift. X-ray absorbance spectroscopy (XAS) has proven to be a powerful method to monitor iron-sulfur clusters in different environments (*12*).

In XAS, high-intensity X-rays are used to selectively excite core electron transitions for specific atoms (*13*). The excitation is selective because the energies required for core electronic transitions are particular to individual atoms. When the X-ray energy matches or exceeds the binding energy of a core electron, the electron is promoted to unpopulated

energy levels or dissociated, creating a sharp absorption edge feature (Figure 2). Analysis of different regions of the X-ray absorption spectrum yields different types of information. XANES (X-ray Absorption Near Edge Structure) refers to energy range immediately before and after the excitation edge, and can provide information on the electronics and geometry of an absorbing atom, such as oxidation state, covalency, and site symmetry. EXAFS (Extended X-ray Absorption Fine Structure) refers to the energy range above the absorption edge, where the ejected electron behaves as a photoelectron wave with a sinusoidal oscillation. EXAFS can provide geometric information, and is particularly known for delivering highly accurate metal-ligand bond lengths, with an accuracy of 0.01-0.02 Å (*13*). Edges are named according to the orbital from which an electron is excited: K-edge refers to the excitation of 1s core electrons, while L-edge refers to excitation from the 2s orbital.

Rather than excitation into the continuum (dissociation), lower energy pre-edge transitions are also possible in XAS. Solomon *et al.* have demonstrated that a pre-edge feature in sulfur K-edge XANES can provide valuable information about the electronic structure of 4Fe4S clusters (*14*). The edge transition in sulfur K-edge spectra corresponds to sulfur 1s → 4p excitation. In iron-sulfur clusters, a lower energy sulfur 1s (S_{1s}) to Fe-based 3d (Fe_{3d}) transition is possible, but is electric-dipole disallowed as a *gerade* (*g*) → *g* transition. However, the sulfur 1s → sulfur 3p transition is electric-dipole allowed as a *g* → *ungerade* transition. Therefore, if sulfur 3p orbitals mix with Fe 3d orbitals, the pre-edge transition ($S_{1s} \rightarrow Fe_{3d}$) becomes partially allowed and gains intensity. This Fe-S covalency can be quantified as the area under the pre-edge transition. In this way, the intensity of the pre-

edge feature at 2470 eV in sulfur K-edge XAS spectra (Figure 2) is a direct measure of the Fe-S covalency in iron-sulfur clusters (*14*).

Solomon *et al.* have used the intensity of the pre-edge feature in sulfur K-edge XANES to study the origin of electronic differences between HiPIPs, which are generally more buried within the protein fold, and ferredoxins, where the clusters are typically more solvent-accessible (*14*). HiPIPs, where the $[4Fe4S]^{3+/2+}$ redox couple is physiologically accessible, show higher intensity of the pre-edge feature, indicating greater Fe-S covalency, than ferredoxins, where the $[4Fe4S]^{2+/+}$ couple is accessible. Hydration was found to be a major determinant of Fe-S covalency, whereas hydrogen bonding from the peptide backbone has a relatively small effect. When a ferredoxin was lyophilized, removing solvent waters, the Fe-S covalency increases significantly, whereas when the protein fold of a HiPIP was denatured, making the cluster more solvent accessible, the covalency decreases (*14*). Solomon *et al.* conclude that the electrostatic effect of water hydrogen-bonding to sulfur ligands decreases Fe-S covalency, weakening Fe-S bonds, and destabilizing the oxidized state of the cluster. Thus ferredoxins (HiPIPs), with their lower (higher) Fe-S covalencies, are prone to reduction (oxidation) at physiological potentials. In addition to the effect of local hydrogen-bonding, the remaining contribution to the observed potentials is proposed to derive from non-local electrostatics.

Furthermore, a series of model $[Fe_4S_4(SR)_4]^{2-}$ complexes with different thiolate ligands (R) was prepared and their sulfur K-edge XAS and electrochemistry measured (*14*). Plotting the Fe-S covalency versus the $[Fe_4S_4]^{3+/2+}$ oxidation potential revealed a linear

correlation (Figure 3). The positive slope indicates that with increasing covalency, the $[Fe_4S_4]^{2+}$ cluster is more easily oxidized. This would in turn correspond to a lower $[Fe_4S_4]^{3+/2+}$ redox potential. Overall, this study showed that the Fe-S covalency measured by XAS is able to quantitatively probe the electrostatic environment of iron-sulfur clusters (*14*).

Here, we use sulfur K-edge XANES to measure the Fe-S covalency of the 4Fe4S cluster of WT *E. coli* EndoIII alone and in the presence of DNA, both in solution and in lyophilized samples. We correlate the changes in covalency with a shift in redox potential, in order to obtain molecular evidence for the decrease in redox potential upon DNA binding that was observed electrochemically. An increase in Fe-S covalency would be expected upon the DNA binding of EndoIII.

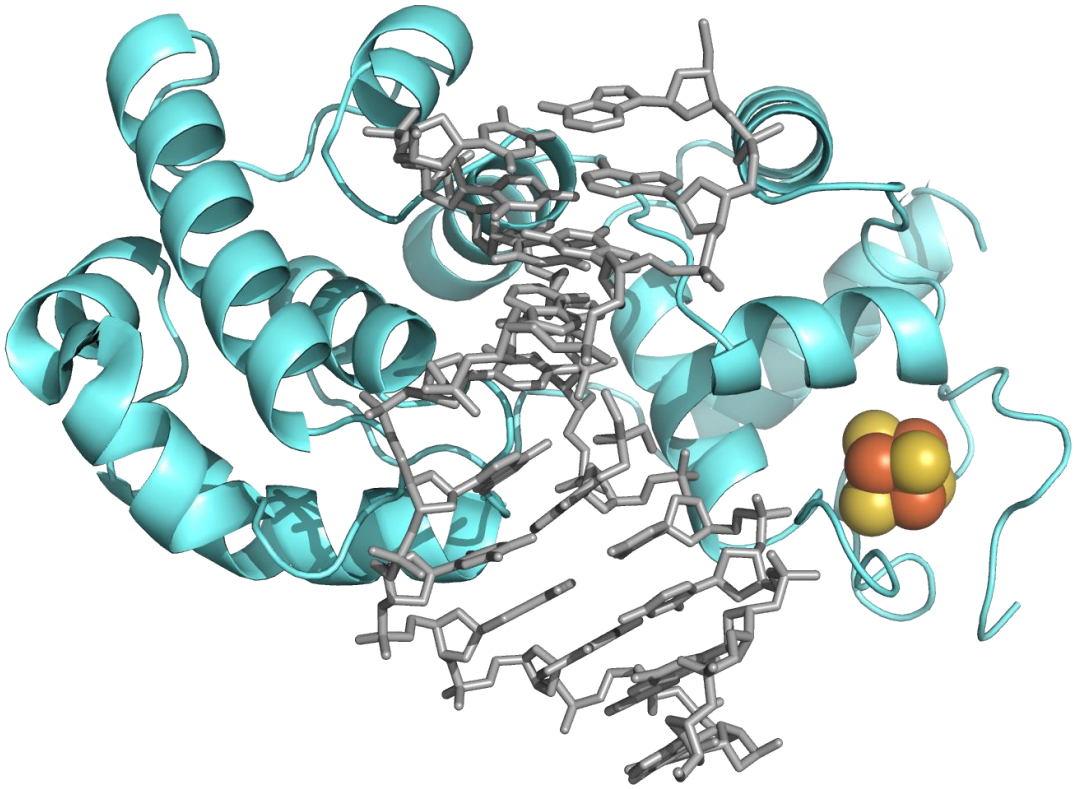

Figure 1. Crystal structure of the 4Fe4S cluster-containing base excision repair protein Endonuclease III bound to DNA. PDB: 2ABK with DNA from 1ORN. References: Thayer, M.M. et al. *EMBO J.* **1995**, *14*, 4108-4120; Fromme, J.C. et al. *EMBO J.* **2003**, *22*, 3461-3471.

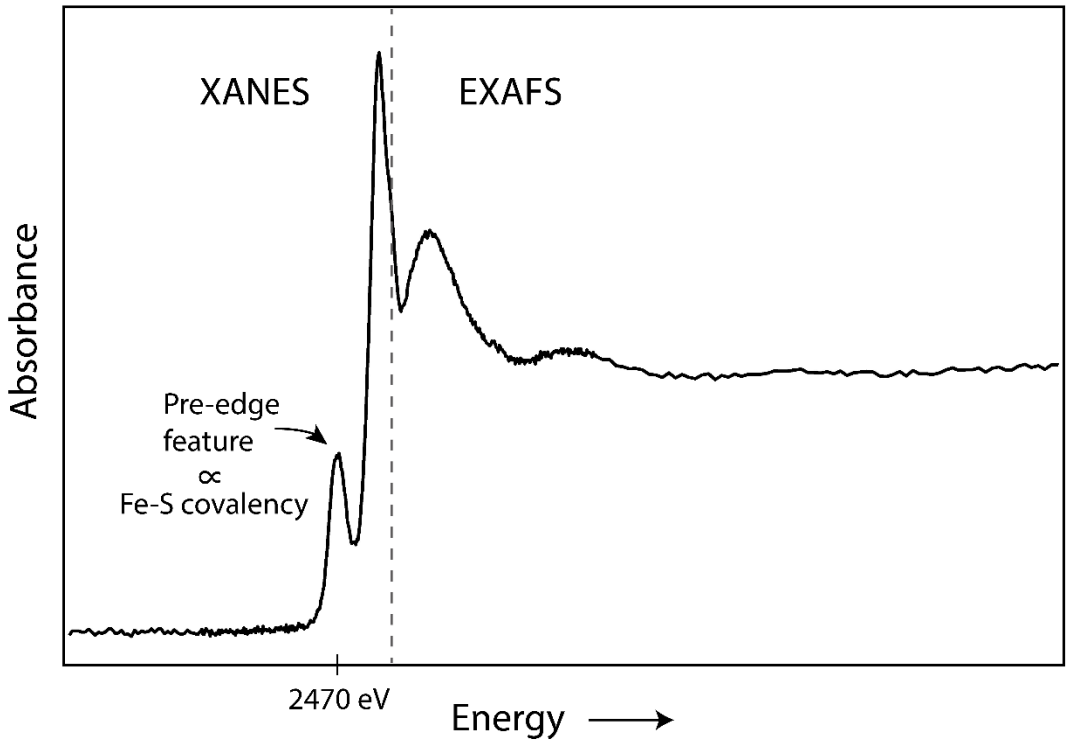

Figure 2. Sulfur K-edge X-ray absorbance spectra showing sharp absorption edge that appears with increasing X-ray energy. XANES refers to the energy range around the absorption edge, whereas EXAFS focuses on the oscillations of the ejected electron at higher energies. The spectra of EndoIII in solution is shown. The intensity of the pre-edge feature at 2470 eV is proportional to the Fe-S covalency of 4Fe4S clusters, which can be correlated to their redox potential.

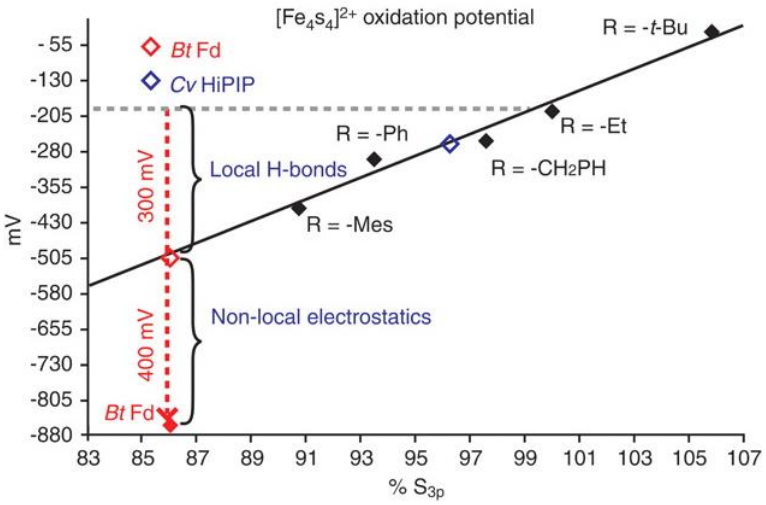

Figure 3. Plot of Fe-S covalency as a function of $[Fe_4S_4]^{2+}$ oxidation potential for a series of $[Fe_4S_4(SR)_4]^{2-}$ complexes with different thiolate ligands (R) (black diamonds). Shown relative to the model complex with R = Et, which has been assigned 100% covalency. Open diamonds represent predicted oxidation potential values based on covalency. From Dey et al. *Science* **2007**, *318*, 1464-1468. Reprinted with permission from AAAS.

5.2 Experimental section

5.2.1 Expression and purification of EndoIII

WT *E. coli* EndoIII was overexpressed in BL21star-(DE3)pLysS cells containing a pET11-ubiquitin-His_6-*nth* construct and purified as detailed previously (*15*), with the exception that the final buffer contained 10% glycerol, rather than 20% glycerol (20 mM sodium phosphate, pH 7.5, 0.5 mM EDTA, 150 mM NaCl, 10% glycerol). EndoIII in this 10% glycerol buffer is stable overnight stored at 4°C, but is less stable in the absence of glycerol; therefore glycerol was not removed until the day of sample preparation. On the day of sample preparation, glycerol was removed from half the volume of protein solution using HiPrep 26/10 desalting column (GE Healthcare) equilibrated with a buffer containing 20 mM sodium phosphate, pH 7.5, 0.5 mM EDTA, 150 mM NaCl. Next, the protein solutions either containing 10% glycerol or no glycerol were separately concentrated. First, 10,000 MWCO Amicon Ultra 15 mL centrifugation filter units (Millipore) were used to concentrate each protein solution to 1 mL or less. Finally, 10,000 MWCO Amicon Ultra 0.5 mL centrifugation filter units (Millipore) were used to concentrate the protein solutions until very dark colored, to approximately 300 µL each if using an entire protein preparation from 6 L of bacterial culture.

5.2.2 Sample preparation

DNA strands were purchased from Integrated DNA Technologies (a 20-mer mixed sequence strand: 5′-GTGAGCTAACGTGTCAGTAC-3′ and its complement). DNA strands (5 µmol) were resuspended in MilliQ water (200 µL, divided into 100 µL aliquots)

and purified by ethanol precipitation. Briefly, 1000 µL of cold 200 proof ethanol, followed by 50 µL of 3 M NaCl were added to the 100 µL DNA solutions and vortexed; the DNA should precipitate. Solutions were then frozen in liquid nitrogen for approximately 5 minutes and spun at 16,000 RCF to pellet the DNA. Finally, the supernatant was removed and the pellet dried on a speed-vac. When dried, the strands were resuspended in 20 mM sodium phosphate, pH 7.5, 0.5 mM EDTA, 150 mM NaCl, either with 10% glycerol or lacking glycerol and quantified based on calculated ε_{260} values for the strands (Integrated DNA Technologies) of 197,800 $M^{-1}cm^{-1}$ for the 20-mer strand and 190,200 $M^{-1}cm^{-1}$ for its complement. Annealing of the strands to form duplexed DNA was accomplished by combining equimolar amounts of the single-stranded DNAs, heating at 90°C for 5 minutes, and slow cooling to room temperature. Separate duplex solutions were prepared in either 10% glycerol or no glycerol buffer.

On the same day as glycerol removal from half of the EndoIII protein solution, and after concentration of the separate 10% glycerol and no glycerol protein solutions, a 4Fe4S cluster loading ratio was calculated for each solution. This calculation is based on the characteristic UV-Visible absorbance at 410 nm of 4Fe4S clusters (Figure 4). To calculate a loading ratio, the concentration of each solution was measured by two separate methods: using ε_{410} = 17,000 $M^{-1}cm^{-1}$, which is specific to the presence of 4Fe4S clusters, and using the Bradford assay, which measures total protein content irrespective of the presence of an iron-sulfur cluster. The 4Fe4S cluster loading ratio was then calculated as: [Protein concentration

based on A_{410}] / [Protein concentration based on Bradford assay] * 100. Typical cluster loading ratios for WT EndoIII were 70-75%.

Finally, to prepare the samples, concentrated solutions of EndoIII protein were mixed with the DNA duplex at a ratio of 1 mol EndoIII: 20 mol base-pairs DNA. An equivalent volume of buffer was added to EndoIII alone solutions so that for each condition (10% glycerol or no glycerol), identical concentrations of EndoIII solutions were prepared both with and without DNA. Mixtures were allowed to incubate on wet ice for 30 minutes to allow for binding before freezing in liquid nitrogen. No glycerol samples were then placed on a lyophilizer, while solution samples were stored in a -80°C freezer. When the lyophilized samples were dried, both samples were placed on dry ice and sent to Stanford University for XAS measurements.

5.2.3 X-ray absorbance spectroscopy

Lyophilized samples were ground to a fine powder, dispersed as thinly as possible on Kapton tape to minimize possible self-absorption fluorescence effects, and mounted across the window of an aluminum plate. Solution samples were loaded via a syringe into 50 µL Teflon cells with Kapton tape as the back window and 6 µm polypropylene as the front window. Measurements were performed at the Stanford Synchrotron Radiation Laboratory (SSRL) on beam line 4-3. Details of the beamline configuration have been described previously (*12*). A shutter was added between the ionization chamber for incident beam intensity and the sample box in order to decrease photoreduction. The solution samples were measured at a constant temperature of 4°C during data collection using a controlled

flow of He gas, pre-cooled by liquid N_2. The photon energy was calibrated to the maximum of the first pre-edge feature of $Na_2S_2O_3 \cdot 5H_2O$ at 2472.02 eV. Three to five scans were measured on the sample to ensure reproducibility. Raw data were calibrated and averaged using MAVE in the EXAFSPAK package. By using the PySpline program (*16*), the background was subtracted from all spectra by fitting a second-order polynomial to the pre-edge region and subtracting it from the entire spectrum. Normalization of the data was accomplished by fitting a straight line to the post-edge region and normalizing the edge jump to 1.0 at 2490.0 eV. For protein samples which also have sulfur-containing free cysteine and methionine residues, it is also necessary to normalize for the total number of sulfur atoms in the protein. EndoIII has 3 free cysteine residues (not coordinating the 4Fe4S cluster), and 2 methionine residues. Finally, the data were normalized with the 4Fe4S cluster loading ratio that is calculated as described above. The error from background subtraction and normalization is less than 1%. Intensities of the pre-edge features were quantified by fitting the data with pseudo-Voigt line shapes with a fixed 1:1 ratio of Lorentzian to Gaussian contributions, using the EDG_FIT program (*17*). The error from the fitting procedure is less than 1%. The fitted intensities were converted to %S 3p character according to previously described methods (*18*).

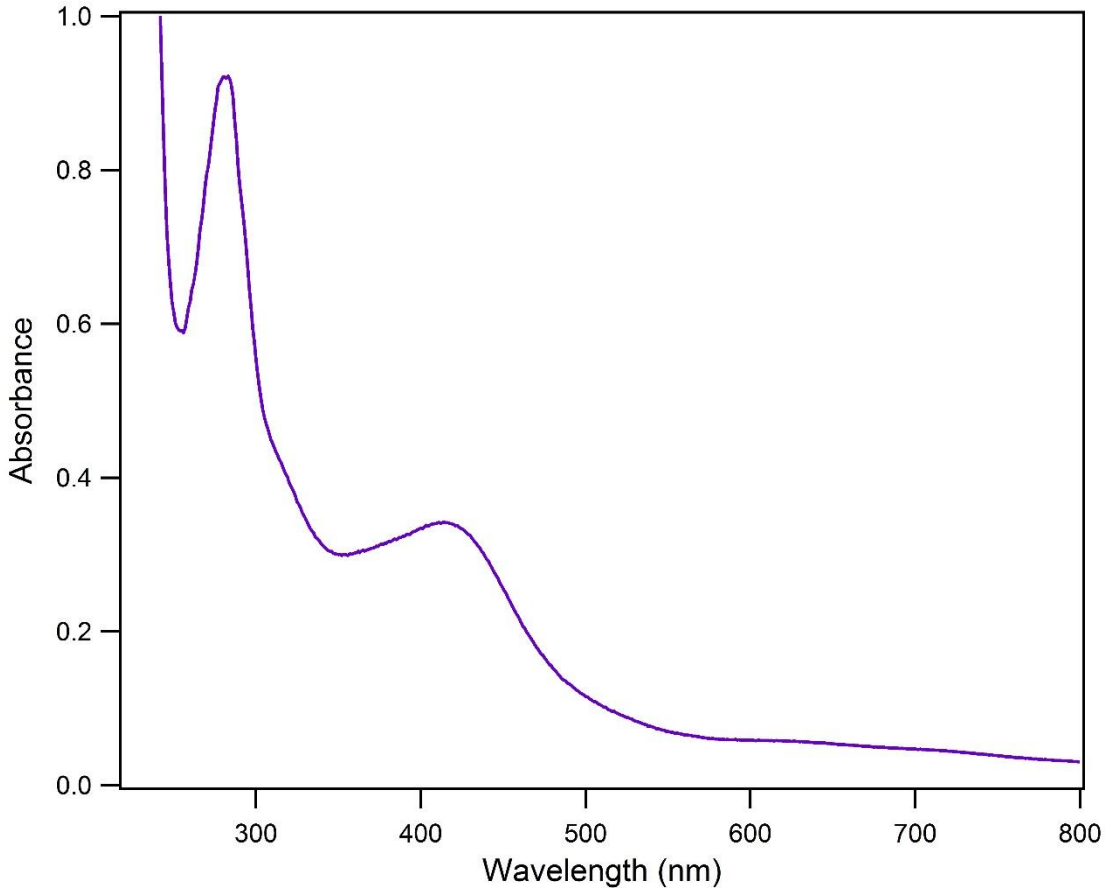

Figure 4. UV-Visible absorbance spectrum of *E. coli* EndoIII showing the shoulder at 410 nm characteristic of a 4Fe4S cluster. Buffer: 20 mM sodium phosphate, pH 7.5, 0.5 mM EDTA, 150 mM NaCl, 20% glycerol.

5.3 Results and discussion

The sulfur K-edge XAS spectra of EndoIII alone and in the presence of a 20-mer mixed sequence DNA duplex (5′-GTGAGCTAACGTGTCAGTAC-3′) at a ratio of 1 mol protein to 20 mol base-pairs was measured both in solution and in samples that had been lyophilized. High protein concentrations (1 mM or greater) are necessary for high quality data. Identical concentrations of EndoIII were compared with and without DNA, for both solution and lyophilized samples. The data were normalized according to a 4Fe4S cluster loading ratio, calculated as the protein concentration based on ε_{410} = 17,000 $M^{-1}cm^{-1}$, specific for the presence of a 4Fe4S cluster, relative to the total protein concentration as measured by the Bradford assay. Typical cluster loading ratios were 70% or greater. The normalized data of the pre-edge $S_{1s} \rightarrow Fe_{3d}$ transition are shown in Figure 5.

For both solution and lyophilized samples, an increase in the area of the pre-edge feature was observed upon DNA binding, indicating an increase in Fe-S covalency. This result is consistent with a negative shift in the redox potential of the $[4Fe4S]^{3+/2+}$ couple of EndoIII upon DNA binding, as we have observed electrochemically (*4*). A larger increase in covalency upon DNA binding is observed with solution samples, indicating that hydration is an important factor. DNA binding shifts the cluster into a more buried, less solvent-accessible environment. In lyophilized samples, where solvent has been removed, we still observe an increase in Fe-S covalency upon DNA binding: this can likely be attributed to the non-local electrostatics of the DNA poly-anion. Additionally, lower Fe-S covalency is observed upon lyophilization for both EndoIII alone and EndoIII with DNA samples. This

decrease in covalency upon lyophilization is also evident with HiPIP from *C. vinosum* (unpublished observations).

While quantitation is still preliminary, the EndoIII with DNA sample in solution has the same covalency (100% S_{3p}) as the reference model complex $[Fe_4S_4(SEt)_4]^{2-}$ in the work of Solomon *et al.* (*14*). In the EndoIII alone sample, the covalency is decreased to 93% relative to the model complex. Based on the slope that defines the relationship between covalency and $[4Fe4S]^{3+/2+}$ oxidation potential, this 7% difference would correspond to an approximately 150 mV decrease in the redox potential of the $[4Fe4S]^{3+/2+}$ couple of EndoIII upon binding DNA, remarkably similar to that observed electrochemically. The absolute values of the $[4Fe4S]^{3+/2+}$ potentials do not fall along the line in Figure 3, likely due to non-local electrostatics.

This result has been reproduced in two separate trials. In a third trial, a smaller decrease in Fe-S covalency was observed upon EndoIII binding DNA. However, in this trial, no difference was observed between the lyophilized and solution samples, suggesting that the samples had been damaged in some way. Therefore data from this trial was deemed not reliable.

Sheila David and co-workers have also participated in this collaboration, performing similar studies with the homologous 4Fe4S cluster-containing BER protein MutY (data not shown). Similar results were obtained for both EndoIII and MutY. An increase in Fe-S covalency upon DNA binding is observed for both solution and lyophilized samples that indicates a negative shift in the redox potential of the $[4Fe4S]^{3+/2+}$ cluster of MutY in the

presence of DNA. Furthermore, lower Fe-S covalency is observed upon lyophilization for both MutY alone and MutY with DNA samples, as with EndoIII. Overall, the trend of increasing Fe-S covalency upon DNA binding is consistent: (*i*) in duplicate trials, (*ii*) with both EndoIII and MutY, and (*iii*) with our previously observed DNA electrochemistry results.

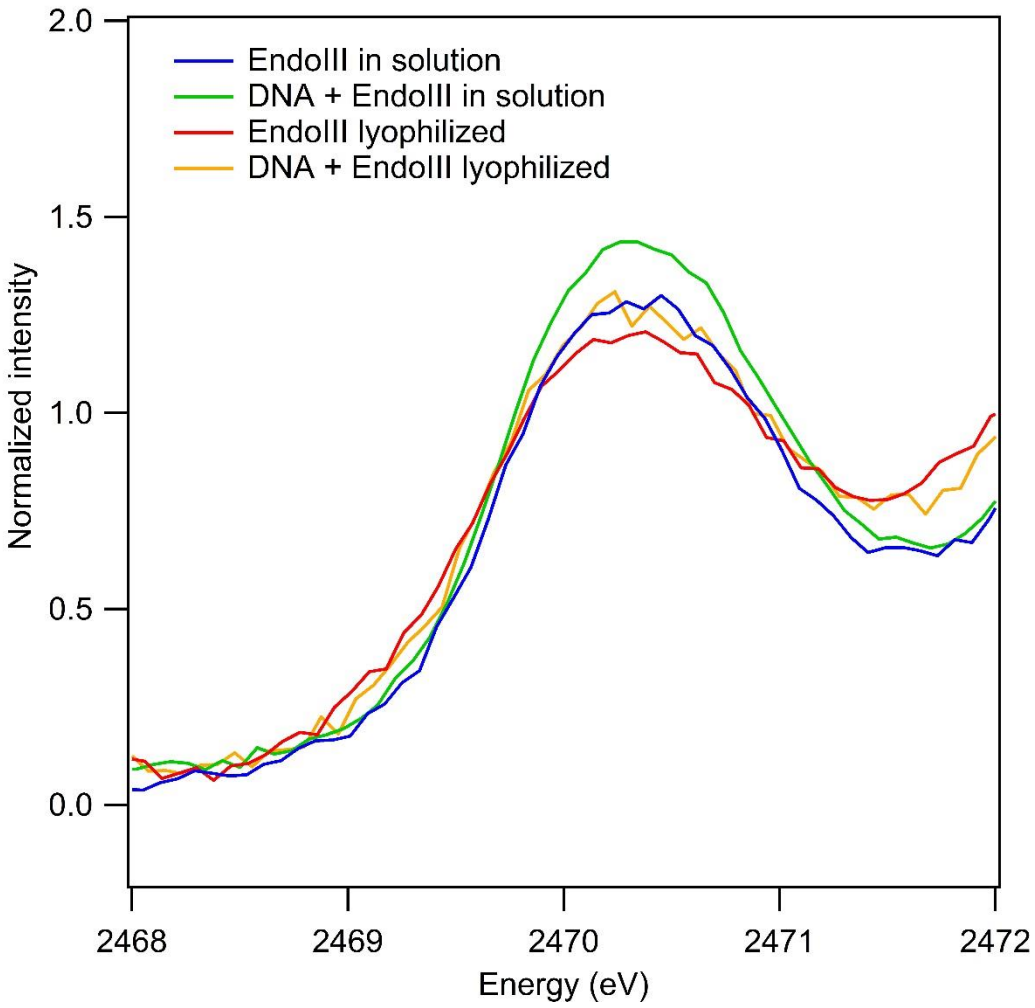

Figure 5. Sulfur K-edge XAS spectra of EndoIII alone and in the presence of a 20-mer mixed sequence DNA duplex (1 mol protein: 20 mol base-pairs), both in solution and lyophilized. Sequence of duplex: 5′-GTGAGCTAACGTGTCAGTAC-3′. Lyophilized samples: 71% cluster loading; before freezing, concentrations: EndoIII: 1.00 mM (based on A_{410}), 1.00 mM DNA duplex (20 mM base-pairs). Solution samples: 72% cluster loading; concentrations: EndoIII: 1.25 mM (based on A_{410}), 1.25 mM DNA duplex (25 mM base-pairs). Buffer: 20 mM sodium phosphate, pH 7.5, 150 mM NaCl, 0.5 mM EDTA, either with 10% glycerol (solution samples) or in the absence of glycerol (lyophilized samples).

5.4 Conclusions

Sulfur K-edge XAS can be used to directly probe the iron-sulfur covalency in 4Fe4S clusters via a pre-edge transition that gains intensity if sulfur 3p orbitals mix with Fe 3d orbitals. This Fe-S covalency has been correlated with the redox potential of 4Fe4S clusters, thus allowing quantitative examination of the electrostatic environment of the cluster under different conditions. Here with the 4Fe4S cluster-containing BER protein EndoIII we have reproducibly shown an increase in Fe-S covalency upon DNA binding, both in solution and lyophilized samples. This covalency increase is consistent with a negative shift in the redox potential of the EndoIII $[4Fe4S]^{3+/2+}$ couple of approximately 150 mV upon DNA binding. Thus the shift in Fe-S covalency upon DNA binding as measured by XAS agrees with previous electrochemistry results. Moreover, the same trend is observed in MutY, a homologous 4Fe4S cluster BER protein. Therefore we have obtained direct molecular evidence for the negative shift in the $[4Fe4S]^{3+/2+}$ cluster redox potential of BER proteins upon DNA binding. These data support the feasibility of our model whereby these proteins can utilize DNA charge transport to cooperate in order to efficiently find DNA lesions inside cells.

References

1. Kim, Y.J.; Wilson, D.M. 3rd. Overview of base excision repair biochemistry. *Curr. Mol. Pharmacol.* **2012**, *5*, 3-13.

2. Cunningham, R.P., Asahara, H., Bank, J.F., Scholes, C.P., Salerno, J.C., Surerus, K., Munck, E., McCracken, J., Peisach, J., and Emptage, M.H. Endonuclease III is an iron-sulfur protein. *Biochemistry* **1989**, *28*, 4450-4455.

3. Porello, S.L.; Cannon, M.J.; David, S.S. A substrate recognition role for the [4Fe-4S]$^{2+}$ cluster of the DNA repair glycosylase MutY. *Biochemistry* **1998**, *37*, 6465-6475.

4. Gorodetsky, A.A.; Boal, A.K.; Barton, J.K. Direct electrochemistry of Endonuclease III in the presence and absence of DNA *J. Am. Chem. Soc.* **2006**, *128*, 12082-12083.

5. Muren, N.B.; Olmon, E.D.; Barton, J.K. Solution, surface, and single molecule platforms for the study of DNA-mediated charge transport. *Phys. Chem. Chem. Phys.* **2012**, *14*, 13754-13771.

6. Boal, A.K.; Yavin, E.; Lukianova, O.A.; O'Shea, V.L.; David, S.S.; Barton, J.K. DNA-bound redox activity of DNA repair glycosylases containing [4Fe-4S] clusters. *Biochemistry* **2005**, *44*, 8397-8407.

7. Stephens, P.J.; Jollie, D.R.; Warshel, A. Protein control of redox potentials of iron-sulfur proteins. *Chem. Rev.* **1996**, *96*, 2491-2513.

8. Mui, T.P.; Fuss, J.O.; Ishida, J.P.; Tainer, J.A.; Barton, J.K. ATP-stimulated, DNA-mediated redox signaling by XPD, a DNA repair and transcription helicase. *J. Am. Chem. Soc.* **2011**, *133*, 16378-16381.

9. Grodick, M.A.; Segal, H.M.; Zwang, T.J.; Barton, J.K. DNA-mediated signaling by proteins with 4Fe-4S clusters is necessary for genomic integrity. *J. Am. Chem. Soc.* **2014**, *136*, 6470-6478.

10. Wan, C.; Fiebig, T.; Kelley, S.O.; Treadway, C.R.; Barton, J.K.; Zewail, A.H. Femtosecond dynamics of DNA-mediated electron transfer. *Proc. Natl. Acad. Sci. USA* **1999**, *96*, 6014-6019.

11. Boal, A.K.; Genereux, J.C.; Sontz, P.A.; Gralnick, J.A.; Newman, D.K.; Barton, J.K. Redox signaling between DNA repair proteins for efficient lesion detection *Proc. Natl. Acad. Sci. USA* **2009**, *106*, 15237-15242.

12. Solomon, E.I.; Hedman, B.; Hodgson, K.O.; Dey, A.; Szilagyi, R.K. Ligand K-edge X-ray absorption spectroscopy: covalency of ligand-metal bonds. *Coord. Chem. Rev*. **2005**, *249*, 97-129.

13. Bencze, K.Z.; Kondapalli, K.C.; Stemmler, T.L. X-Ray Absorption Spectroscopy. In *Applications of Physical Methods to Inorganic and Bioinorganic Chemistry*; Scott, R.A. and Lukehart, C.M., Ed.; Wiley, 2007; p. 513-528.

14. Dey, A.; Jenney, F.E. Jr.; Adams, M.W.W.; Babini, E.; Takahashi, Y.; Fukuyama, K.; Hodgson, K.O.; Hedman, B.; Solomon, E.I. Solvent tuning of electrochemical potentials in the active sites of HiPIP versus ferredoxin. *Science* **2007**, *318*, 1464-1468.

15. Pheeney, C.G.; Arnold, A.R.; Grodick, M.A.; Barton, J.K. Multiplexed electrochemistry of DNA-bound metalloproteins. *J. Am. Chem. Soc*. **2013**, *135*, 11869-11878.

16. George, G. N.; Stanford Synchrotron Radiation Laboratory: Menlo Park, CA, 1990.

17. Tenderholt, A. L.; v2.1, Ed.; Stanford University: Stanford, CA, 2007.

18. Sarangi, R.; George, S.D.; Rudd, D.J.; Szilagyi, R.K.; Ribas, X.; Rovira, C.; Almeida, M.; Hodgson, K.O.; Hedman, B.; Solomon, E.I. Sulfur K-Edge X-ray absorption spectroscopy as a probe of ligand–metal bond covalency: Metal vs ligand oxidation in copper and nickel dithiolene complexes. *J. Am. Chem. Soc*. **2007**, *129*, 2316-2326.